Controlling quantum motions of a trapped and driven electron: an exact analytic treatment

2006 J. Phys. A: Math. Gen. 39 401

(http://iopscience.iop.org/0305-4470/39/2/010)

INSTITUTE OF PHYSICS PUBLISHING JOURNAL OF PHYSICS A: MATHEMATICAL AND GENERAL

J. Phys. A: Math. Gen. **39** (2006) 401–415 doi:10.1088/0305-4470/39/2/010

Controlling quantum motions of a trapped and driven electron: an exact analytic treatment

Gengbiao Lu, Wenhua Hai and Qiongtao Xie

Department of Physics, Hunan Normal University, Changsha 410081, People's Republic of China

E-mail: adcve@public.cs.hn.cn

Received 26 August 2005, in final form 13 November 2005
Published 14 December 2005
Online at stacks.iop.org/JPhysA/39/401

Abstract

We consider a harmonically trapped and strongly driven electron in a one-dimensional (1D) quantum wire. A set of exact complete solutions of the time-dependent Schrödinger equation is constructed, which shows the properties of generalized squeezed coherent states. The corresponding probability densities behave like some breathing and oscillating wave-packet-trains. The resonance ladders of the expectation energy are found and the transition probabilities between two stationary states are exactly calculated. The results reveal that the quantum motions of the considered system can be controlled by adjusting the laser driving field.

PACS numbers: 03.65.Ge, 73.22.Dj, 68.65.Fg, 03.65.Db

1. Introduction

Recently, the development of ultrahigh-intensity lasers [1] has led to increasing study of the particles driven by a strong field with high frequency. The process of high-harmonic generation (HHG) due to an intense atom–field interaction has received substantial attention in recent years [2], and harmonically generated coherent x-ray transients have been predicted and indeed are beginning to be observed [3]. In a strong laser field, the stabilization of the system was predicted theoretically [4–6] and has been verified experimentally [7, 8]. We know that the physical phenomena with a strong field are very different from those with a weak field, and the mathematical treatments for the former cannot use the traditional perturbation theory [9]. Therefore, a reliable and accurate theoretical procedure must be developed in the study involving a strong field. For the high-frequency driving fields, the approximate method of Kramers–Henneberger (KH) oscillating frame representation [10] has been employed to effectively describe some physical systems [11–14]. The Floquet theory [15] also had some success in treating the dynamics of the systems. For example, in the treatment of the system with homogeneous oscillating potential $V(t) = V_0 \cos(\omega t)$, the Floquet theory

is straightforward, and has been well studied during the past decade [16]; the time-dependent dipole-type potential, $V(x,t) = eF_1 x\cos(\omega t)$, which appears in some experimental setups has also been investigated by using the Floquet theory [17–19]. The Green's function method was applied to treat the quantum transition of a harmonically trapped particle in the strong external field of the same form [20]. With the loss of validity of perturbation techniques, it is very important to get a set of exact solutions [19, 21–23] for the considered systems. Recently, the studies on the matter wave packet stimulated many people's interest [24], especially in the controlling of the wave packet [25].

In this paper, we consider a 1D harmonically trapped electron interacting with a strong external field in the form $[\varepsilon_0 x + \varepsilon_1 x\cos(\Omega t)]$ [13, 26], and construct a set of exact solutions of the time-dependent Schrödinger equation by the analytical method [21]. We shall apply the analytical solutions to exactly treat some interesting physical problems, such as the properties of generalized squeezed coherent states, resonance ladders of the expectation energies, and quantum transitions between two stationary states. In particular, we will illustrate the controlling of the probability wave-packet-train.

The outline of this paper is as follows. In section 2, we obtain a set of analytic solutions of the system, which describe the probability wave-packet-train consisting of $n+1$ breathing and oscillating packets. We discuss some physical properties making use of the exact quantum states, such as the expectation values of position and momentum, which agree with the classical orbit of a driven oscillator and its classical momentum, respectively. The interesting properties of squeezed coherent states are illustrated, which periodically vary with time. It is shown that the average energy of the electron in the exact quantum states is composed of classical and quantum parts, which is different from the energy of any known coherent state [27]. In section 3, we discuss the quantum transition and resonance ladders via the exact solution. First, we calculate exactly the transition probability between two stationary states under the laser field, and confirm the agreement with Landovitz's result obtained by using the Green's function method [20]. Then we illustrate the average energy for the resonance and non-resonance cases. The resonance ladders of the expectation energy are found, which tell us how the energy evolutes with time in a resonance transition process. In section 4, we discuss how to realize the controlling of a single electron wave-packet-train by using the external field. We seek the relationship between the centre position of the wave-packet-train and controllable parameters, and find that with the increase of the laser frequency, the oscillating amplitudes of the wave packets become smaller and smaller. However, when we increase the intensity of laser field, the oscillating amplitudes become larger and larger. Similarly, the static electric field strength can affect the centre position of the oscillation. Therefore, by adjusting the laser field and static electric field, we can easily control the wave-packet-train theoretically. Finally, in section 5, we make some concluding remarks.

2. Exact quantum states of the trapped and driven electron

We consider a harmonically trapped and strongly driven electron in a one-dimensional (1D) quantum wire along the x direction. The harmonic potential is generated by a magnetic field and the time-dependent dipole-type potential is produced by a laser field [13, 26]. The time-dependent Schrödinger equation governing the motion of the electron reads

$$\mathrm{i}\frac{\partial\Psi}{\partial t} = -\frac{1}{2}\frac{\partial^2\Psi}{\partial x^2} + \frac{1}{2}x^2\Psi + \varepsilon(t)x\Psi, \tag{1}$$

where $\varepsilon(t) = \varepsilon_0 + \varepsilon_1\cos(\Omega t)$ denotes the driving field with ε_0 being the normalized strength of the static electric field, and ε_1 and Ω are the normalized strength and frequency of the laser

field. Let m, C and $\omega = eB/(2Cm)$ be the electron mass, light speed and cyclotron frequency of the magnetic field B, respectively. In equation (1) we have adopted the natural units with $m = \hbar = \omega = 1$ such that the spatial coordinate x and time t are in units of the harmonic oscillator length $\ell = \sqrt{\hbar/(m\omega)}$ and inverse frequency ω^{-1}, the laser frequency is normalized by ω and the magnetic and laser potentials are normalized by $\hbar\omega$, respectively.

Applying the well-known technique for solving the time-dependent Schrödinger equation [21], we construct the $n+1$ exact solutions of equation (1) as (see the appendix)

$$\Psi_n(x,t) = R_n(x,t)\,\mathrm{e}^{\mathrm{i}\Theta_n(x,t)}, \qquad n = 0, 1, 2, 3, \ldots, \tag{2}$$

where the real functions $R_n(x,t)$ and $\Theta_n(x,t)$ read

$$R_n(x,t) = \left(\frac{\sqrt{k_0}}{\sqrt{\pi}2^n n!\rho(t)}\right)^{\frac{1}{2}} H_n(\xi)\exp\left(-\frac{1}{2}\xi^2\right), \tag{3}$$

$$\Theta_n(x,t) = -\left(\frac{1}{2}+n\right)\theta + b_2 x + \frac{\dot{\rho}}{2\rho}x^2 + \frac{1}{2}\int\left(b_1^2 - b_2^2\right)\mathrm{d}t, \tag{4}$$

with $H_n(\xi)$ being the Hermite polynomial of the spacetime variable

$$\xi(x,t) = \frac{\sqrt{k_0}}{\rho(t)}x - \frac{b_1(t)\rho(t)}{\sqrt{k_0}}. \tag{5}$$

In equations (3)–(5), the real functions $\rho(t)$, $\theta(t)$, $b_1(t)$ and $b_2(t)$ have the forms

$$\rho(t) = \sqrt{\varphi_1^2 + \varphi_2^2}, \qquad \theta(t) = \arctan\left(\frac{\varphi_1}{\varphi_2}\right), \tag{6}$$

$$b_1 = \frac{1}{\rho^2}\left[\varphi_1(t)\int^t \varepsilon(t)\varphi_2(t)\,\mathrm{d}t - \varphi_2(t)\int^t \varepsilon(t)\varphi_1(t)\,\mathrm{d}t + b_0^r\varphi_1(t) + b_0^i\varphi_2(t)\right], \tag{7}$$

$$b_2 = \frac{1}{\rho^2}\left[-\varphi_1(t)\int^t \varepsilon(t)\varphi_1(t)\,\mathrm{d}t - \varphi_2(t)\int^t \varepsilon(t)\varphi_2(t)\,\mathrm{d}t + b_0^i\varphi_1(t) - b_0^r\varphi_2(t)\right], \tag{8}$$

where φ_i are the periodic functions, $\varphi_1 = A\cos(t+\alpha)$, $\varphi_2 = B\cos(t+\beta)$, while A, B, α, β, b_0^r, b_0^i and $k_0 = AB\sin(\alpha-\beta)$ are the constants to be determined by the form of the initial state. In order to maintain the independence between φ_1 and φ_2, we need $\alpha \neq \beta$ at any case. It is worth noting that $\rho(t)$ and $\theta(t)$ do not depend on the external potential, and only $b_1(t)$ and $b_2(t)$ are determined by the external potential.

The exact solutions are $n+1$ complete solutions with some arbitrary constants and obey the orthonormalization condition $\langle\Psi_n \mid \Psi_{n'}\rangle = \delta_{n,n'}$. They describe the motion of the trapped and driven single electron. When the different system parameters in a wide range of parameters are taken, we can get some different kinds of quantum states, which can be used to treat various physical problems. For example, when $A = B = \sqrt{k_0}$, $\alpha = 0$ and $\beta = -\frac{\pi}{2}$ are set, we get the wavefunction with $\xi = x - b_1(t)$, that contains the known results reported in [22, 28, 29]. Because of the property of the orthonormalization, the solution in equation (2) can serve as a complete basis to investigate more physical systems, say the Bose–Einstein condensate held in the harmonic potential [21].

According to the property of the Hermite polynomial $H_n(\xi)$, the probability density $R_n^2(x,t)$ describes the wave-packet-trains consisting of $n+1$ Gaussian wave packets. Noticing equation (7), the orbit of the centre of the wave-packet-train $x_c(t)$ is given by setting $\xi = 0$ in equation (5) as

$$x_c(t) = \frac{\rho^2(t)b_1(t)}{k_0} = \frac{1}{k_0}\left[\varphi_1(t)\int^t \varepsilon(t)\varphi_2(t)\,\mathrm{d}t - \varphi_2(t)\int^t \varepsilon(t)\varphi_1(t)\,\mathrm{d}t + b_0^r\varphi_1(t) + b_0^i\varphi_2(t)\right]. \tag{9}$$

This is just the classical orbit of the driven harmonic oscillator. Combining the time functions $\varphi_1(t)$, $\varphi_2(t)$ and $\varepsilon(t)$, we know that the centre of the wave-packet-train oscillates periodically with time. The function $\rho(t)$ in equation (3) can be called the function of width and height of the wave-packet-train [21]. When $\alpha = 0$, $\beta = -\pi/2$, $A = B$ are set, $\rho(t)$ is a constant, which means that the width and height of the wave-packet-train do not change with time. In the other case, the function $\rho(t)$ periodically varies with time that will cause the corresponding changes of the widths and heights of wave-packet-train, which is identified with the so-called breathing of wave packets [30].

Combining equation (2) with equations (3)–(5), we get the initial states of the system as

$$\Psi_n(x,0) = \left(\frac{\sqrt{k_0}}{\sqrt{\pi}2^n n!\rho(0)}\right)^{\frac{1}{2}} H_n[\xi(x,0)]\,\mathrm{e}^{-\frac{1}{2}\xi^2(x,0)}\,\mathrm{e}^{\mathrm{i}\Theta_n(x,0)}, \qquad n = 0, 1, 2, 3, \ldots. \tag{10}$$

In equation (10), when the parameters are selected as $\alpha = 0$, $\beta = -\frac{\pi}{2}$, $A = B = 1$, $b_0^i = 0$, $b_0^r = \frac{\varepsilon_1}{2}$ (resonance case) and $b_0^r = \frac{\varepsilon_1}{1-\Omega^2}$ (non-resonance case), we get $\rho(0) = \sqrt{k_0} = 1$ and $b_1(0) = b_2(0) = 0$ from equations (6)–(8), which lead to the initial state becoming the well-known energy-eigenstate $\Psi_n(x,0) = \psi_n(x)$ of a harmonic oscillator. Obviously, the case $n = 0$, $\rho(0) = \sqrt{k_0} = 1$ and $b_1(0) \neq 0$ implies $\Psi_0(x,0) = \psi_0(x - b_1(0))$ to be the usual coherent state. The same parameters and nonzero n mean that the initial states are generalized coherent states with multiple wave packets, which contain rich information for different parameters.

Now we calculate the expectation values of the coordinate and momentum under the exact quantum states of equation (2). Applying the relationships between the exact quantum states [21]

$$\begin{aligned}
&\xi\Psi_n = \sqrt{\frac{n}{2}}\,\mathrm{e}^{-\mathrm{i}\theta}\Psi_{n-1} + \sqrt{\frac{n+1}{2}}\,\mathrm{e}^{\mathrm{i}\theta}\Psi_{n+1},\\
&2\xi^2\Psi_n = \sqrt{n(n-1)}\,\mathrm{e}^{-2\mathrm{i}\theta}\Psi_{n-2} + (2n+1)\Psi_n + \sqrt{(n+1)(n+2)}\,\mathrm{e}^{2\mathrm{i}\theta}\Psi_{n+2},\\
&\frac{1}{H_n}\frac{\partial H_n}{\partial\xi}\Psi_n = 2n\frac{H_{n-1}}{H_n}\Psi_n = \sqrt{2n}\,\mathrm{e}^{-\mathrm{i}\theta}\Psi_{n-1}
\end{aligned} \tag{11}$$

and employing Dirac's symbols, ket and bra, we can easily arrive at the expectation values

$$\begin{aligned}
&\bar{x} = \langle\Psi_n \mid \hat{x} \mid \Psi_n\rangle = \frac{\rho^2(t)b_1(t)}{k_0},\\
&\bar{p} = \langle\Psi_n \mid \hat{p} \mid \Psi_n\rangle = b_2(t) + b_1(t)\dot{\rho}(t)\rho(t)/k_0 = \dot{\bar{x}},\\
&\bar{x}^2 = \langle\Psi_n \mid \hat{x}^2 \mid \Psi_n\rangle = k_0^{-1}\rho^2(t)\left[n + \frac{1}{2} + \frac{\rho^2(t)b_1^2(t)}{k_0}\right],\\
&\bar{p}^2 = \langle\Psi_n \mid \hat{p}^2 \mid \Psi_n\rangle = \left[\frac{\dot{\rho}^2(t)}{k_0} + \frac{k_0}{\rho^2(t)}\right]\left(n + \frac{1}{2}\right) + b_2^2(t)\\
&\qquad\qquad + \frac{b_1^2(t)\dot{\rho}^2(t)\rho^2(t)}{k_0^2} + \frac{2b_1(t)b_2(t)\dot{\rho}(t)\rho(t)}{k_0}.
\end{aligned} \tag{12}$$

Interestingly, we find that the expectation value of position in equation (12) is equal to the centre coordinate of the wave-packet-train in equation (9), and the expectation momentum is its time derivative. Therefore, the expectation 'quantum orbit' agrees with the corresponding classical orbit, which demonstrates a good classical-quantum correspondence.

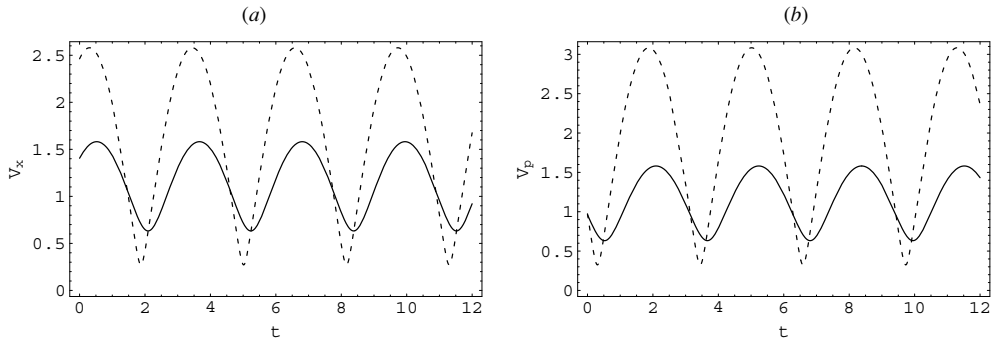

Figure 1. The time evolution of squeezed parameters for (a) the position squeezed parameter and (b) the momentum squeezed parameter. The solid lines are associated with the parameters $n = 0$, $A = 2$, $B = 5$, $\alpha = \pi/3$ and $\beta = -\pi/6$, and the dashed lines correspond to the parameters $n = 0$, $A = 1$, $B = 7$, $\alpha = \pi/6$ and $\beta = -\pi/10$. The spacetime variables x and t are normalized in units of ℓ and ω^{-1}.

From equation (12) we get the variations of position and momentum as

$$\begin{aligned} \triangle x(t) &= (\overline{x^2} - \bar{x}^2)^{\frac{1}{2}} = \frac{\rho(t)}{\sqrt{k_0}}\sqrt{n+\frac{1}{2}}, \\ \triangle p(t) &= (\overline{p^2} - \bar{p}^2)^{\frac{1}{2}} = \sqrt{\left[\frac{\dot{\rho}^2(t)}{k_0} + \frac{k_0}{\rho^2(t)}\right]}\sqrt{n+\frac{1}{2}}. \end{aligned} \tag{13}$$

It is well known [27] that for the dimensionless x and p the energy eigenstates of a harmonic oscillator are associated with $\triangle x = \triangle p = \sqrt{n+\frac{1}{2}}$, and under the coherent state of the harmonic oscillator we have $\triangle x = \triangle p = \frac{1}{\sqrt{2}}$. From equation (13), we find that under the exact states in equation (2) of the driven harmonic oscillator, $\triangle x$ and $\triangle p$ vary with time. However, they are independent of the time-dependent external field, since the function $\rho(t)$ governing their time evolutions does not depend on the external field. Note that a state is called a squeezed state [31] if the variations satisfy $\triangle x < \frac{1}{\sqrt{2}}$ or $\triangle p < \frac{1}{\sqrt{2}}$. Letting the squeezing parameter be $V_s(t) = \sqrt{2}\triangle S(t)$ for $(S = x, p)$, we define the instantaneous squeezing states which obey $V_S(t) < 1$ at some time t. The time-dependent squeezing property is illustrated in figure 1. In figure 1, we see the periodical behaviour of the squeezing parameter V_s. The oscillating amplitude is determined by the parameters A and B, and the oscillating phase depends on the parameters α and β. When we adjust the system constants A, B, α, β, we can get a series of interesting squeezed coherent states, and the squeezing parameters V_s periodically vary with time and depend on the amplitudes and phases. Given equation (13), the Heisenberg uncertainty relation becomes

$$\triangle x(t)\triangle p(t) = \sqrt{\left[\frac{\dot{\rho}^2(t)\rho^2(t)}{k_0^2} + 1\right]}\left(n+\frac{1}{2}\right) \geqslant \left(n+\frac{1}{2}\right). \tag{14}$$

This general relation contains the harmonic case $\triangle x(t)\triangle p(t) = \left(n+\frac{1}{2}\right)$ for the parameters $\alpha = 0, \beta = -\frac{\pi}{2}, A = B$. When $n = 0$ and $\rho =$ constant are set, from equation (14) we arrive at the minimum uncertainty of the usual coherent state, namely $\triangle x(t)\triangle p(t) = \frac{1}{2}$. The conclusion about the squeezed coherent state is similar to the result in [32, 33].

The phase $\Theta_n(x, t)$ of the wavefunction in equation (4) is a complicated time-space function, which is directly related to the average energy of the system. We now calculate

the average energy under the quantum-mechanical definition [27], $E_n = \langle \Psi_n \mid \mathrm{i}\frac{\partial}{\partial t} \mid \Psi_n \rangle = -\langle \Psi_n \mid \dot{\Theta}_n \mid \Psi_n \rangle$. Combining equations (6)–(8) and (12), we get the expectation value of energy

$$E_n = \left(\frac{k_1}{k_0}\right)\left(n + \frac{1}{2}\right) + \frac{\bar{p}^2}{2} + \frac{\bar{x}^2}{2} + \bar{x}\varepsilon(t), \tag{15}$$

where $k_1 = \left[\dot{\rho}^2(t) + k_0^2/\rho^2(t) + \rho^2(t)\right]/2$ is a constant. It is quite interesting that the time-dependent average energy in equation (15) is composed of classical and quantum parts, which is different from the expectation energy of the known coherent state [27]. The time-dependent external field can influence the classical part of average energy, since the former contains the external potential $\varepsilon(t)$. However, the external field does not affect the quantum part of the energy. From equation (15) we easily get the adjacent energy level spacing $\triangle E = E_{n+1} - E_n = \left(\frac{k_1}{k_0}\right)$, which is a constant determined by the system parameters k_0 and k_1. When we take the parameters as $\alpha = 0, \beta = -\frac{\pi}{2}, A = B = 1$, to make $k_0 = k_1 = 1$, the quantum level becomes the well-known one of the stationary state harmonic oscillator, $\triangle E = 1(\hbar\omega)$. In the viewpoint of quantum mechanics, the electron can transit between the different quantum states, and this will be discussed in detail as follows.

3. Transition probabilities and energy ladders

For simplicity, we do not consider the effect of the static electric field to the transition probability. When the zero static electric field is considered, the system becomes a harmonic oscillator interacting with a laser field $V(x, t) = x\varepsilon_1 \cos(\Omega t)$. Applying such a field to the above-mentioned formulae, we directly get the exact quantum states of the system. For a weak laser field with small strength we know that the quantum transition can be treated approximately by using the quantum perturbation theory [27]. When the laser field is strong enough, we cannot use the traditional perturbation theory and must seek the effective non-perturbation methods, such as the Green's function method [20] and the exact-solution method. In fact, once the exact solutions are given, we can directly calculate the transition probabilities between the stationary states. To do this, we expand the exact quantum states $\Psi_n(x, t)$ by adopting the energy eigenstates of harmonic oscillator as

$$\Psi_n(x, t) = \sum_m C_{n,m}(t)\psi_m(x). \tag{16}$$

As an example, we take the parameter set as $\alpha = 0, \beta = -\frac{\pi}{2}, A = B = 1, b_0^i = 0, b_0^r = \frac{\varepsilon_1}{2}$ (resonance case), and $b_0^r = \frac{\varepsilon_1}{1-\Omega^2}$ (non-resonance case) so that equations (6)–(8) give $\rho = 1, b_1(0) = b_2(0) = 0$, and the initial state $\Psi_n(x, 0)$ just becomes the energy eigenstate of harmonic oscillator

$$\Psi_n(x, 0) = \psi_n(x) = N_n H_n(x) \exp\left[-\tfrac{1}{2}x^2\right], \tag{17}$$

where x is the dimensionless coordinate and $N_n = \left(\frac{1}{\sqrt{\pi}2^n n!}\right)^{\frac{1}{2}}$ is the normalization constant. After multiplying both sides of equation (16) by $\psi_{m'}(x)$, we integrate this equation to obtain the transition amplitude from state n to state m as

$$C_{n,m}(t) = \int_{-\infty}^{+\infty} \mathrm{d}x\ \psi_m^*(x)\Psi_n(x, t), \tag{18}$$

with the initial value $C_{n,m}(0) = \delta_{n,m}$. In the computation, the orthnormalization condition of equation (17), $\int_{-\infty}^{+\infty} \psi_{m'}(x)\psi_m(x)\,\mathrm{d}x = \delta_{m,m'}$, has been employed. Consequently, the corresponding transition probability reads

$$P_{n,m}(t) = |C_{n,m}(t)|^2. \tag{19}$$

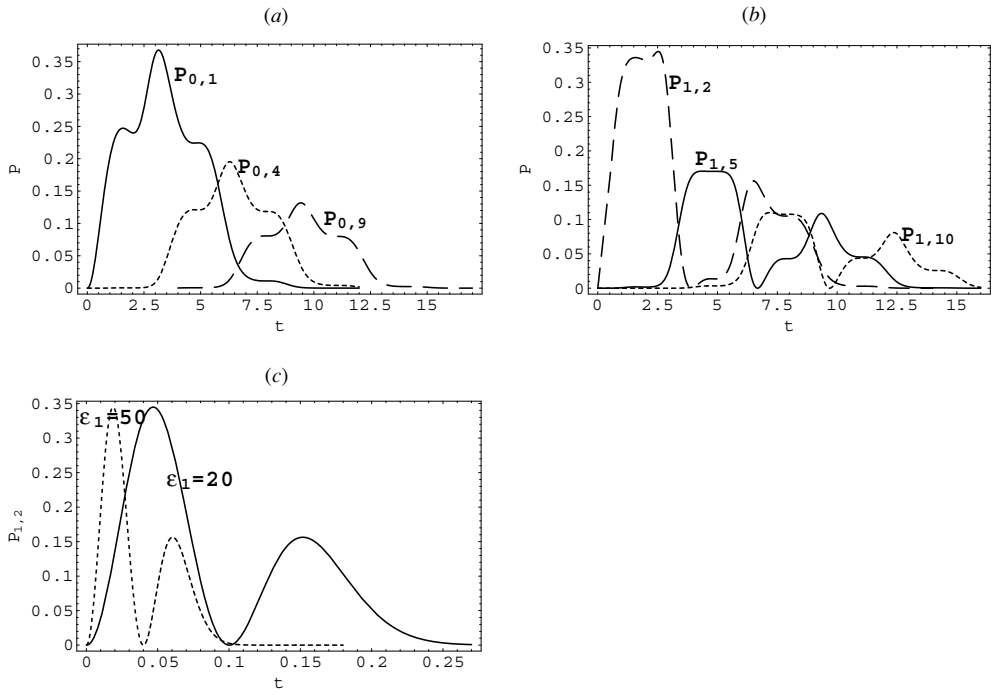

Figure 2. (*a*) The time evolutions of transition probabilities from equations (2), (17), (18) and (19) for the resonance case $\Omega = 1(\omega)$ with the laser strength $\varepsilon_1 = 0.9$. The solid line expresses the probability $P_{0,1}(t)$ from $n = 0$ state to $m = 1$ state. The dotted line and long-dashed line represent $P_{0,4}(t)$ and $P_{0,9}(t)$, respectively. (*b*) The corresponding results $P_{n,m}(t)$ for $n = 1, m = 2, 5, 10$ and the same parameters as in (*a*). (*c*) The transition probability $P_{1,2}(t)$ for two different values of laser strengths. The solid line is associated with $\varepsilon_1 = 20$, and the dotted line with $\varepsilon_1 = 50$. The spacetime variables x and t are normalized in units of ℓ and ω^{-1}, and the laser potential $\varepsilon_1 x$ is normalized in units of $\hbar\omega$.

By applying the exact solution in equation (2) with the initial state $\Psi_n(x, 0) = \psi_n(x)$ to equations (18) and (19), we can exactly compute the transition probability $P_{n,m}(t)$ induced by the time-dependent laser field.

For the resonance case $\Omega = 1(\omega)$, the numerical results are shown in figures 2(*a*) and (*b*), where the laser strength is taken as $\varepsilon_1 = 0.9$. In figure 2(*a*) the transition probability $P_{0,1}(t)$ indicated by the solid line shows that its peak corresponds to the time $t = \pi$. The plots of probabilities $P_{0,4}(t)$ and $P_{0,9}(t)$ indicate the time associated with their peak values to be $t = 2\pi$ and $t = 3\pi$. However, when $n = 1$ is considered, the time corresponding to the probability peaks shows small deviations from the integer times of π, as in figure 2(*b*). In figure 2(*c*), we show the transition probability $P_{1,2}(t)$ for the stronger laser fields. The solid curve corresponds to $\varepsilon_1 = 20$ and the dotted curve to $\varepsilon_1 = 50$. All these plots show that the transition probabilities $P_{n,m}(t)$ tend to zero as $t \to \infty$. In particular, when we increase the laser strength as in figure 2(*c*), the curves are translated towards the left and the transition probabilities approach zero earlier. The very small $P_{n,m}(t)$ and the normalization condition $\sum_{m=1}^{\infty} P_{n,m}(t) = 1$ mean that all the infinite components in the state of equation (16) cannot be neglected at $t = \infty$ for the resonance case. Simultaneously, the resonance leads the centre position in equation (9) of the wave-packet-train to infinity, indicating the loss of stability. The resonance loss of stability is therefore the reason of the transition from the initial state to any

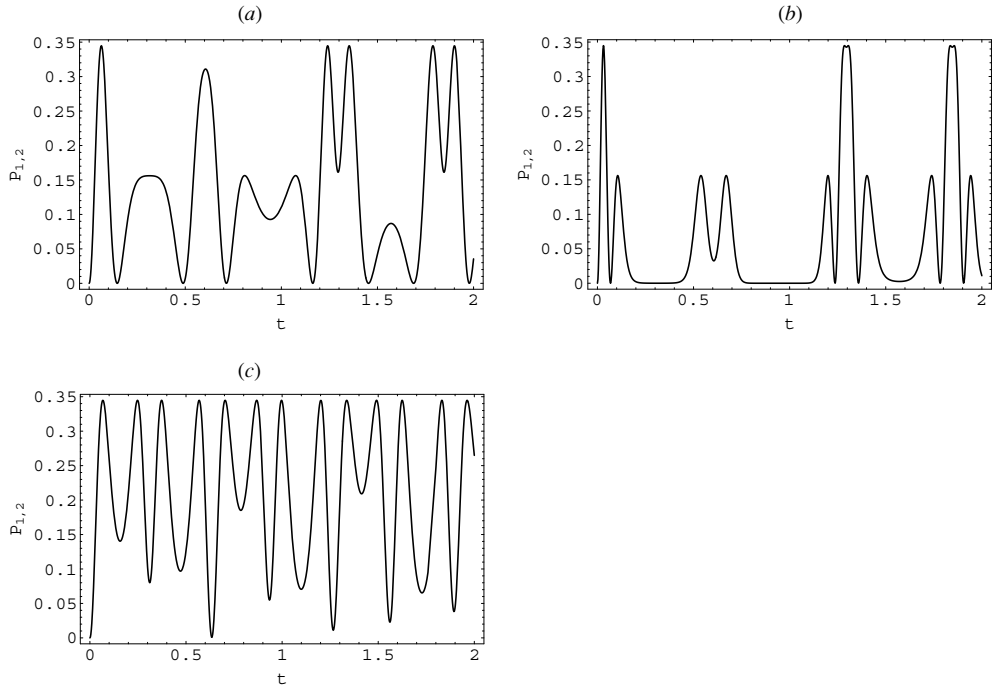

Figure 3. The time evolution of transition probability $P_{1,2}(t)$ in the non-resonance case for the parameters (*a*) $\Omega = 5$, $\varepsilon_1 = 15$; (*b*) $\Omega = 5$, $\varepsilon_1 = 30$ and (*c*) $\Omega = 10$, $\varepsilon_1 = 15$. The same units as in figure 2 are used.

final state. These results approximately agree with the corresponding results obtained by the Green's function method [20]. Although there may be some small differences between them, our results from the exact solution are more accurate. In particular, the comparison between our exact results and that from quantum perturbation theory shows that the selection rule [27] $\Omega - \omega = \pm 1(\omega)$ of transitions is no longer valid for the strong field case.

For the non-resonance case $\Omega \neq 1(\omega)$, we can also directly calculate the transition probabilities with our exact solutions. In figure 3, we plot the transition probability $P_{1,2}(t)$ for the different laser frequencies and amplitudes. The results of the non-resonance case indicate that the transition probability $P_{1,2}(t)$ periodically evolves and never permanently vanishes all the time. For the larger laser strengths, the maxima of transition probabilities can reach the value of the resonance peaks in figure 2. This is an important multiphoton effect. A comparison between figures 3(*a*) and (*c*) shows that using the larger frequency difference $\Omega - \omega$ can produce more probability peaks.

We now numerically illustrate the average energy from equation (15) for the given parameters below equation (16). Inserting such parameters and resonance frequency $\Omega = 1(\omega)$ into equations (6)–(8), (12) and (15) produces $\rho^2 = k_0 = 1$, $\bar{x} = b_1(t) = \frac{1}{2}\varepsilon_1[\cos t - \cos^3 t - \sin t(t + \sin t \cos t)]$, $\bar{p} = \dot{\bar{x}} = -\frac{1}{2}\varepsilon_1(t \cos t + \sin t)$ and $E_n(t) = n + 0.5 + \varepsilon_1^2(0.0625 + 0.125t^2 - 0.0625\cos(2t) - 0.125t\sin(2t))$. In figure 4, we plot the time evolutions of average energies E_0 and E_1 for (*a*) the resonance case and (*b*) the non-resonance case, respectively. In the resonance case, we find that there exist some interesting plateaus of the energy curves as in figure 4(*a*), which are similar to the spatial ladders of the Wannier–Stark potential [34]. The centres of energy ladders appear at $t = \pi k$ for $k = 0, 1, 2, 3, \ldots$, where

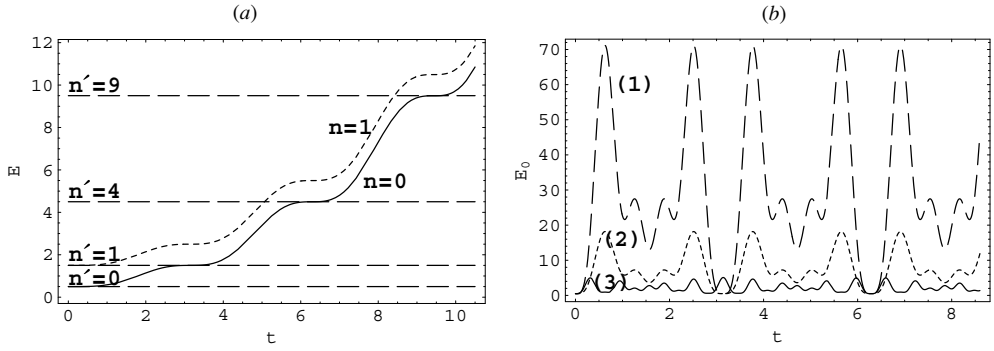

Figure 4. (*a*) The time evolution of average energy for the resonance case with parameters $\Omega = 1, \varepsilon_1 = 0.9$. The solid line stands for the average energy $E_0(t)$ of ground state, the dotted line denotes the average energy $E_1(t)$ of first excited state and the long-dashed lines indicate the centres of energy ladders, $E_0(\pi k) = 0.5 + k^2$, which appear at $t = \pi k$ for $n' = k^2, k = 0, 1, 2, 3, \ldots$. (*b*) The ground-state energy $E_0(t)$ of thenon-resonance case with parameters (1) $\Omega = 5, \varepsilon_1 = 30$; (2) $\Omega = 5, \varepsilon_1 = 15$; (3) $\Omega = 10, \varepsilon_1 = 15$. The same units as in figure 2 are used.

$\dot{E}_n(t) = \frac{1}{4}\varepsilon_1^2 t[1 - \cos(2t)] = 0$. The resonance ladders of average energy are caused by the classical part of equation (15); however, the energy values of the plateaus centres satisfy the quantized relationship $E_n(\pi k) = n + 0.5 + 0.125\pi^2 k^2 \varepsilon_1^2$ for $k = 1, 2, 3, \ldots$. From this formula we can see that when the laser strength is set as $\varepsilon_1 = \sqrt{8}/\pi$, the values of energy ladders obey $E_n(\pi k) = n + 0.5 + k^2$ for $t = \pi k$ with $k = 0, 1, 2, 3, \ldots$. In figure 4(*a*) we show the instances of $\varepsilon_1 = \sqrt{8}/\pi \approx 0.9$ for $n = 0, 1$. In the non-resonance case $\Omega \neq 1(\omega)$, the average energy periodically varies with time as in figure 4(*b*). A comparison between figures 4(*a*) and (*b*) exhibits that in both cases there may exist the local minima of average energy appearing at the times $t = \pi k$ for $k = 0, 1, 2, 3, \ldots$. But only in the resonance case does the energy unceasingly increase with time, which leads to the energy ladders and the possible transitions between the ladders. Combining figure 4(*a*) with figure 2(*a*) shows that for the initial ground state the centres of energy ladders correspond to the maxima of transition probabilities.

It is interesting for us to analytically investigate the relationship between the transition probability and average energy. This relationship can be easily obtained by substituting the wavefunction of equation (16) into the formula of average energy,

$$\begin{aligned} E_n &= \langle \Psi_n(x,t) \mid \hat{H} \mid \Psi_n(x,t) \rangle \\ &= \sum_m \left(m + \frac{1}{2}\right) P_{n,m}(t) + \frac{\varepsilon_1 \cos(\Omega t)}{\sqrt{2}} \sum_m C_{n,m}(t) \\ &\quad \times \sum_{m'} C_{n,m'}(t)(\sqrt{m'}\delta_{m,m'-1} + \sqrt{m'+1}\delta_{m,m'+1}). \end{aligned} \tag{20}$$

This form differs from that of equation (15). It exhibits the relationship between the average energy and transition probability more clearly than the latter. For example, it points out the possibility that the resonance ladders of average energies do not exactly correspond with the local maxima of transition probabilities for the $n \neq 0$ case. This conclusion agrees with the numerical results given in figures 2(*b*) and 4(*a*).

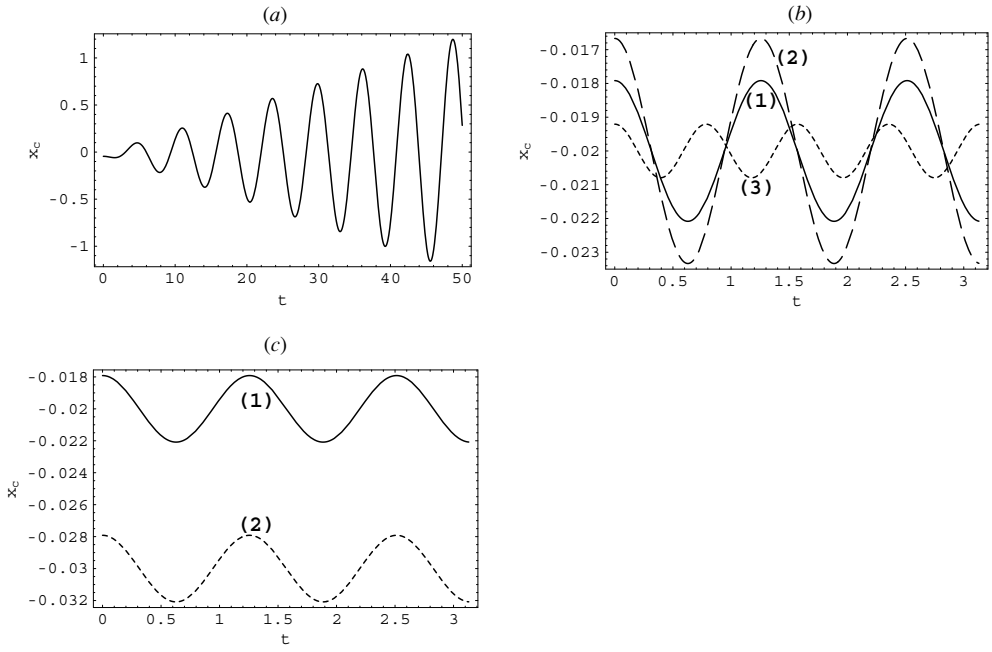

Figure 5. (*a*) The time evolution of centre position x_c of wave-packet-train for the resonance case $\Omega = 1(\omega)$, where $\varepsilon_0 = 0.02, \varepsilon_1 = 0.05$. (*b*) The time evolution of x_c in the non-resonance case for the parameter sets (1) $\Omega = 5, \varepsilon_0 = 0.02, \varepsilon_1 = 0.05$; (2) $\Omega = 5, \varepsilon_0 = 0.02, \varepsilon_1 = 0.08$ and (3) $\Omega = 8, \varepsilon_0 = 0.02, \varepsilon_1 = 0.05$. (*c*) The time evolution of x_c in the non-resonance case for (1) $\Omega = 5, \varepsilon_0 = 0.02, \varepsilon_1 = 0.05$ and (2) $\Omega = 5, \varepsilon_0 = 0.03, \varepsilon_1 = 0.05$. The same units as in figure 2 are used.

4. Controlling the wave-packet-train of the system

The control of the wave-packet-train has an important meaning for controlling the motion of the electron and performing the quantum computations [25]. In this section, we discuss how to realize the control of the single electron wave-packet-train by adjusting the external field parameters. We know that the exact solution (2) represents a single electron wave-packet-train, and the centre position x_c of the wave-packet-train is described by equation (9). The external field parameters $(\varepsilon_0, \varepsilon_1, \Omega)$ implied in equation (9) can affect the motion of the centre of wave-packet-trains. To illustrate the effect of the external field on the wave-packet-train, the numerical results are shown in figures 5 and 6. In figure 5, we display the time evolution of centre orbit of the wave-packet-train for different external field parameters. For simplicity, we have taken the solution constants as $b_0^r = b_0^i = 0, \alpha = 0, \beta = -\frac{\pi}{2}, k_0 = 1, A = B = 1$.

In figure 5(*a*) we show the resonance motion of the centre orbit x_c, where the oscillating amplitude becomes larger and larger. The resonance will lead to the loss of stability and the occurrence of transitions between different states. For the non-resonance case as in figures 5(*b*) and (*c*), we find that the centre orbit x_c oscillates periodically with time. By curves (1) and (2) of figure 5(*b*) we illustrate that increasing the laser strength ε_1 will lead to the increase of the amplitude. The comparison between curves (1) and (3) of figure 5(*b*) exhibits that the increase of frequency Ω can decrease the amplitude and period of the orbit x_c. In figure 5(*c*), we give the time evolution of centre position of the wave-packet-train for the different electric field strengths ε_0. The comparison between curves (1) and (2) exhibits that the equilibrium positions

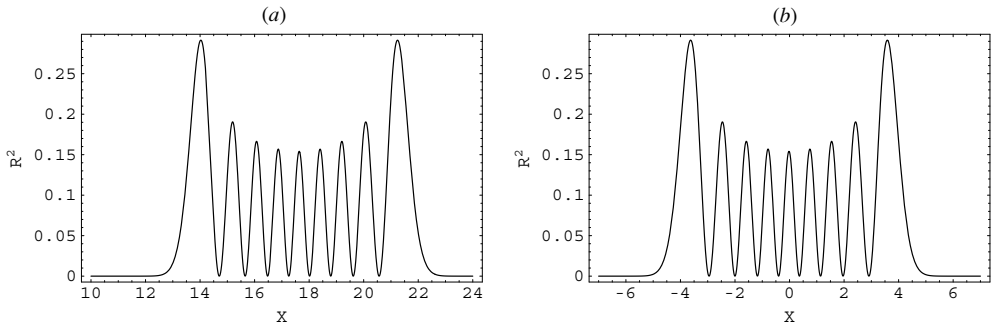

Figure 6. The spatial distribution of the probability density at the time $t = \frac{\pi}{4}$. The external field parameters are set as $(a)\ \Omega = 1.001$, $\varepsilon_0 = 0.02$, $\varepsilon_1 = 0.05$ and $(b)\ \Omega = 100$, $\varepsilon_0 = 0.02$, $\varepsilon_1 = 0.05$. The same units as in figure 2 are used.

x_e of the wave-packet oscillation depend on the values of electric field strength, which just obey $x_e = -\varepsilon_0$. Thus we can control the amplitude, period and equilibrium positions of the wave-packet oscillations by adjusting the external field parameters $(\Omega, \varepsilon_1, \varepsilon_0)$.

We now investigate the dependence of the spatial distribution of the probability density $R^2(x, t)$ on the external field parameters. From figure 5 we have seen that for a set of different parameters the centre positions of the wave-packet-train may be different at a fixed time. In figure 6, we plot the spatial distribution for two different laser frequencies at $t = \frac{\pi}{4}$. The comparison between figures 6(*a*) and (*b*) shows that increasing the frequency causes the translation of the wave-packet-train $R^2\left(x, \frac{\pi}{4}\right)$ towards the left for the considered time. Similar translations can occur when the strength ε_1 or ε_0 is changed. However, in any case the shape of the wave-packet-train is kept. Therefore, by using the external fields we can control only the position of the wave-packet-train. Such control, of course, is useful for performing the quantum logic operations [25, 36].

5. Discussion and conclusion

In summary, we have studied a harmonically trapped and strongly driven electron in a 1D quantum wire. By using the exact complete solutions of the system, we revealed the feature of generalized squeezed coherent states in which there exists the classical-quantum correspondence between the classical orbit and quantum expectation orbit. The spacetime evolutions of probability densities showed a breathing and oscillating wave-packet-train. It is illustrated numerically and analytically that the oscillation amplitude, frequency and equilibrium position of the wave-packet-train can be controlled by adjusting the external fields. Given the exact solution, we calculated exactly the transition probabilities between two stationary states that result in small improvement to the results of Landovitz by using the Green's function technique [20]. The time evolution of average energy in the transition process was illustrated for the resonance and non-resonance cases. The numerical plots exhibit the resonance ladders of the expectation energy, which are similar to the spatial ladders of the Wannier–Stark potential [34]. The centres of energy ladders correspond to some local maxima of the transition probability and some quantum levels of the stationary state harmonic oscillator.

The resonance ladders of energy depend on the laser strength and interaction time, which hint to us how to control the resonance transitions accurately and timely. For example,

figures 2(*a*) and 4(*a*) indicate that for the initial ground state the centres of energy ladders correspond to the maxima of transition probabilities. Therefore, one can realize the transitions from the ground state of a harmonic oscillator with energy $E_0 = 0.5$ to the excitation states with $E_{k^2} = 0.5 + k^2$ for $k = 1, 2, \ldots$, by turning on the laser of strength $\varepsilon_1 \approx 0.9$ at $t = 0$ and turning off it at $t = \pi k$. Once the laser is turned off, the energy of equation (15) becomes an invariant such that the system is kept in the final state. If the interactions are set in succession and the interaction time $\triangle t$ satisfies $\pi \leqslant \triangle t < 2\pi$, the quantum transitions will occur one after another, respectively from state $n = 0$ to $n = 1$, from $n = 1$ to $n = 2$ and so on. This seems to be in agreement with the usual transition rule of the harmonic oscillator. Such control is probably helpful for performing the quantum computations [25, 36].

Finally we note that the solution and the results based on it can be easily extended to the case of harmonically confined and strongly driven ions in a 1D Paul trap [36–38], where such results may be checked experimentally.

Acknowledgments

This work was supported by the National Natural Science Foundation of China under grant nos 10575034 and 10275023, and by the Laboratory of Magnetic Resonance and Atomic and Molecular Physics of China under grant no. T152504.

Appendix. Derivation of the exact solution

Following [21], we set the test solution of equation (1) as

$$\Psi_n = a_n(t) H_n(\xi) \exp[b(t)x - c(t)x^2 - f^2(t)/2], \qquad \xi = e(t)x - f(t), \tag{A.1}$$

where $a(t)$, $b(t)$ and $c(t)$ are the complex functions of time and $e(t)$, $f(t)$ are the real ones. Applying equation (A.1) to equation (1), we get

$$e^2 \frac{\partial^2 H_n(\xi)}{\partial \xi^2} + 2[(be - \mathrm{i}\dot{f}) + (\mathrm{i}\dot{e} - 2ec)x]\frac{\partial H_n(\xi)}{\partial \xi} + [2(2c^2 - \mathrm{i}\dot{c} - 1/2)x^2 + 2(\mathrm{i}\dot{b} - 2bc - \varepsilon(t))x + 2(\mathrm{i}\dot{a}_n/a_n - \mathrm{i}f\dot{f} - c + b^2/2)]H_n(\xi) = 0. \tag{A.2}$$

Comparing this with the Hermite equation $\frac{\partial^2 H_n}{\partial \xi^2} - 2\xi \frac{\partial H_n}{\partial \xi} + 2nH_n = 0$ yields

$$2\mathrm{i}\dot{c} = 4c^2 - 1, \tag{A.3}$$

$$\mathrm{i}\dot{e} = 2ce - e^3, \tag{A.4}$$

$$\mathrm{i}\dot{b} = 2bc + \varepsilon(t), \tag{A.5}$$

$$be = e^2 f + \mathrm{i}\dot{f}, \tag{A.6}$$

$$\mathrm{i}\frac{\dot{a}_n}{a_n} = \mathrm{i}f\dot{f} + c - b^2/2 + ne^2. \tag{A.7}$$

Equation (A.3) is a complex Riccati one, which is associated with the harmonic oscillator equation

$$\ddot{\varphi} = -\varphi, \tag{A.8}$$

through the function transformation $c = \frac{\dot{\varphi}}{2\mathrm{i}\varphi}$. Let the real and imaginary parts of φ be φ_1 and φ_2, respectively. They satisfy equation (A.8) and possess the similar solutions

$$\varphi_1 = A\cos(t + \alpha), \tag{A.9}$$

$$\varphi_2 = B\cos(t + \beta), \tag{A.10}$$

where A, B, α and β are the constants related to the initial conditions of system. Therefore, the general solution of equation (A.8) reads

$$\varphi = \varphi_1 + \mathrm{i}\varphi_2 = \rho(t)\,\mathrm{e}^{\mathrm{i}\theta(t)}, \tag{A.11}$$

where

$$\rho(t) = \sqrt{\varphi_1^2 + \varphi_2^2}, \tag{A.12}$$

$$\theta(t) = \arctan\left(\frac{\varphi_2}{\varphi_1}\right). \tag{A.13}$$

Going back to the function transformation between c and φ produces

$$c = \frac{\dot{\varphi}}{2\mathrm{i}\varphi} = \frac{\dot{\theta}}{2} - \mathrm{i}\frac{\dot{\rho}}{2\rho}. \tag{A.14}$$

Substituting equation (A.11) into equation (A.8) yields the equations of the amplitude and phase as

$$\ddot{\theta} = -\frac{2\dot{\theta}\dot{\rho}}{\rho}, \tag{A.15}$$

$$\ddot{\rho} = \rho\dot{\theta}^2 - \rho, \tag{A.16}$$

with the first integration constants

$$k_0 = \rho^2\dot{\theta} = \varphi_1\dot{\varphi}_2 - \varphi_2\dot{\varphi}_1 = AB\sin(\alpha - \beta), \tag{A.17}$$

$$k_1 = \left(\dot{\rho}^2 + \frac{k_0^2}{\rho^2} + \rho^2\right)\Big/2. \tag{A.18}$$

Substituting equation (A.14) into equation (A.4), we get

$$e(t) = \frac{\sqrt{k_0}}{\rho} = \sqrt{\dot{\theta}}. \tag{A.19}$$

We have set the function $e(t)$ as a real function, so the constant k_0 in equation (A.19) is a positive one. Inserting equation (A.14) into equation (A.5), we arrive at the complex function

$$b = b_1 + \mathrm{i}b_2 = \frac{1}{\varphi}\left[-\mathrm{i}\int \varepsilon(t)\varphi\,\mathrm{d}t + b_0\right], \tag{A.20}$$

where b_1 and b_2 are the corresponding real and imaginary parts of b. Also dividing b_0 into the real part b_0^r and imaginary part b_0^i, and applying equations (A.9)–(A.11), we obtain

$$\begin{aligned} b_1 &= \frac{1}{\rho^2}\left[\varphi_1(t)\int \varepsilon(t)\varphi_2(t)\,\mathrm{d}t - \varphi_2(t)\int \varepsilon(t)\varphi_1(t)\,\mathrm{d}t + b_0^r\varphi_1(t) + b_0^i\varphi_2(t)\right] \\ &= \frac{1}{\rho^2}AB\cos(t+\alpha)\left\{\varepsilon_0\sin(t+\beta) + \frac{\varepsilon_1\sin[(1-\Omega)t+\beta}{2(1-\Omega)} + \frac{\varepsilon_1\sin[(1+\Omega)t+\beta]}{2(1+\Omega)}\right\} \\ &\quad + \frac{1}{\rho^2}b_0^r A\cos(t+\alpha) - \frac{1}{\rho^2}AB\cos(t+\beta) \\ &\quad \times \left\{\varepsilon_0\sin(t+\alpha) + \frac{\varepsilon_1\sin[(1-\Omega)t+\alpha]}{2(1-\Omega)} + \frac{\varepsilon_1\sin[(1+\Omega)t+\alpha]}{2(1+\Omega)}\right\} + \frac{1}{\rho^2}b_0^i B\cos(t+\beta), \end{aligned} \tag{A.21}$$

$$b_2 = \frac{1}{\rho^2}\left[-\varphi_1(t)\int^t \varepsilon(t)\varphi_1(t)\,\mathrm{d}t - \varphi_2(t)\int^t \varepsilon(t)\varphi_2(t)\,\mathrm{d}t + b_0^i\varphi_1(t) - b_0^r\varphi_2(t)\right]$$
$$= -\frac{1}{\rho^2}AB\cos(t+\alpha)\left\{\varepsilon_0\sin(t+\alpha) + \frac{\varepsilon_1\sin[(1-\Omega)t+\alpha]}{2(1-\Omega)} + \frac{\varepsilon_1\sin[(1+\Omega)t+\alpha]}{2(1+\Omega)}\right\}$$
$$-\frac{1}{\rho^2}b_0^r B\cos(t+\beta) - \frac{1}{\rho^2}AB\cos(t+\beta)$$
$$\times\left\{\varepsilon_0\sin(t+\beta) + \frac{\varepsilon_1\sin[(1-\Omega)t+\beta]}{2(1-\Omega)} + \frac{\varepsilon_1\sin[(1+\Omega)t+\beta]}{2(1+\Omega)}\right\} + \frac{1}{\rho^2}b_0^i A\cos(t+\alpha). \tag{A.22}$$

Because $f(t)$ is a real function, we easily derive the result

$$f = \frac{b_1}{e} = \frac{\rho(t)b_1}{\sqrt{k_0}}, \tag{A.23}$$

$$\dot{f} = eb_2 = \frac{\sqrt{k_0}b_2(t)}{\rho(t)} \tag{A.24}$$

from equations (A.6), (A.19) and (A.20). The relationship between equations (A.23) and (A.24) indicates that $\frac{\mathrm{d}}{\mathrm{d}t}\left(\frac{b_1(t)}{e(t)}\right) = e(t)b_2(t)$, which is just in agreement with equations (A.17)–(A.22).

Finally, integrating equation (A.7), we directly get

$$a_n = \frac{A_n}{\sqrt{\rho}}\exp\left[-\mathrm{i}\left(n+\frac{1}{2}\right)\theta + \frac{\mathrm{i}}{2}\int\left(b_1^2 - b_2^2\right)\mathrm{d}t\right], \tag{A.25}$$

where A_n is a constant to be determined from the normalization condition. Inserting equations (A.14), (A.19)–(A.25) into equation (1) leads to the exact solution (2) with equation (3), where the normalization condition $\int|\Psi|^2\,\mathrm{d}x = 1$ for giving the constant $A_n = [\sqrt{k_0}/(\sqrt{\pi}2^n n!)]^{1/2}$ has been used.

References

[1] Guimaräes P *et al* 1993 *Phys. Rev. Lett.* **70** 3792
[2] Protopapus M, Paulus D G and Knight P L 1997 *Phys. Rev. Lett.* **79** 4550
Kazamias S, Douillet D, Weihe F, Valentin C, Rousse A, Sebban S, Grillon G, Aug F, Hulin D and Balcou Ph 2003 *Phys. Rev. Lett.* **90** 193901
[3] Corkum P B 2000 *Nature* **403** 845
[4] Gavrila M and Kaminski J Z 1984 *Phys. Rev. Lett.* **52** 613
[5] Pont M, Walet N R, Gavrila M and McCurdy C W 1988 *Phys. Rev. Lett.* **61** 939
Pont M and Gavrila M 1990 *Phys. Rev. Lett.* **65** 2362
[6] Burnett K, Knight P L, Piraux B R M and Reed V C 1991 *Phys. Rev. Lett.* **66** 301
[7] de Boer M P, Hoogenraad J H, Vrijen R B, Constantinescu R C, Noordam L D and Muller H G 1994 *Phys. Rev.* A **50** 4085
[8] Reinhold C O, Burgdörfer J, Frey M T and Dunning F B 1997 *Phys. Rev. Lett.* **79** 5226
[9] Simon B 1991 *Bull. Am. Math. Soc.* **24** 303 and references therein
[10] Kramers H A 1956 *Quantum Mechanics* (Amsterdam: North-Holland)
Henneberger W C 1968 *Phys. Rev. Lett.* **21** 838
[11] Gavrila M (ed) 1992 *Atom in Intense Laser Field* (New York: Academic) and references therein
[12] Protopapas M, Keitel C H and Knight P L 1997 *Rep. Prog. Phys.* **60** 389 and references therein
[13] Vorobeichik I and Moiseyev N 1999 *Phys. Rev.* A **59** 1699
Vorobeichik I and Moiseyev N 1999 *Phys. Rev.* A **59** 2511
[14] Gomez Llorente J M and Plata J 1992 *J. Phys. A: Math. Gen.* **25** L303

[15] Shirley J H 1965 *Phys. Rev.* **138** B979
[16] Li W and Reichl L E 1999 *Phys. Rev.* B **60** 15732 and references therein
[17] Perez C *et al* 1999 *Phys. Rev.* A **59** 3701
Vorobeichik I *et al* 1998 *Europhys. Lett.* **41** 111
Vorobeichik I *et al* 1999 *Phys. Rev.* A **59** 1699
Vorobeichik I *et al Phys. Rev.* A **59** 2511
[18] Wanger M 1996 *Phys. Rev. Lett.* **76** 4010
Wanger M 1997 *Phys. Rev.* B **55** R10217
Wanger M 1997 *Phys. Rev.* B **57** 11899
[19] Li W and Reichl L E 2000 *Phys. Rev.* B **62** 8269
[20] Landovitz L F 1975 *Phys. Rev.* A **11** 67
[21] Hai W, Huang S and Gao K 2003 *J. Phys. B: At. Mol. Opt. Phys.* **36** 3055
Hai W, Lee C and Chong G 2004 *Phys. Rev.* A **70** 053621
Hai W, Xie Q and Fang J 2005 *Phys. Rev.* A **72** 012116
Hai W, Zhu X, Feng M, Shi L, Gao K and Fang X 2001 *J. Phys. A: Math. Gen.* **34** L79
[22] Truscott W S 1993 *Phys. Rev. Lett.* **70** 1900
[23] Wagner M 1996 *Phys. Rev. Lett.* **76** 4010
[24] Maeda H and Gallagher T F 2004 *Phys. Rev. Lett.* **92** 133004
Hughes S 2004 *Phys. Rev.* B **69** 205308
Niilura H, Villeneuve D M and Corkum P B 2004 *Phys. Rev. Lett.* **92** 133002
Lee K F, Villeneuve D M, Corkum P B and Shapiro E A 2004 *Phys. Rev. Lett.* **93** 233601
[25] Shapiro E A, Spanner M and Ivanov M Y 2003 *Phys. Rev. Lett.* **91** 237901
[26] Peremolov A M and Popov V S 1969 *Teor. Mat. Fiz.* **1** 360
[27] Zeng J 2000 *Quantum Mechanics* 3rd edn (Beijing: Science Press)
[28] Büttiker M and Landauer R 1982 *Phys. Rev. Lett.* **49** 1739
[29] Banter Y M, Usmani O and Nazarov Y V 2004 *Phys. Rev. Lett.* **93** 136802
[30] Schrade G, Man'ko V I, Schleich W P and Glauber R J 1995 *Quantum Semiclass. Opt.* **7** 307
[31] Ramon G, Brif C and Mann A 1998 *Phys. Rev.* A **58** 2506
[32] Lostelecky V A, Nieto M M and Truax D R 1993 *Phys. Rev.* A **48** 1045
[33] Aliaga J, Crespo G and Proto A N 1990 *Phys. Rev.* A **42** 618
[34] Glück M, Kolovsky A R and Korsch H J 1999 *Phys. Rev. Lett.* **83** 891
[35] Gu Y 1992 *Quantum Chaos* (ShangHai: ShangHai Science-Education Press)
[36] Poyatos J F, Cirac J I and Zoller P 1998 *Phys. Rev. Lett.* **81** 1322
[37] Leibfried D, Blatt R, Monroe C and Wineland D 2003 *Rev. Mod. Phys.* **75** 281
[38] Hai W, Feng M, Zhu X, Shi L, Gao K and Fang X 1999 *J. Phys. A: Math. Gen.* **32** 8265